Metal–Organic Frameworks

DOI: 10.1002/anie.201310276

Pressure-Induced Bond Rearrangement and Reversible Phase Transformation in a Metal–Organic Framework**

Elinor C. Spencer, Mangalampalli S. R. N. Kiran, Wei Li, Upadrasta Ramamurty,* Nancy L. Ross, and Anthony K. Cheetham**

Abstract: *Pressure-induced phase transformations (PIPTs) occur in a wide range of materials. In general, the bonding characteristics, before and after the PIPT, remain invariant in most materials, and the bond rearrangement is usually irreversible due to the strain induced under pressure. A reversible PIPT associated with a substantial bond rearrangement has been found in a metal–organic framework material, namely [tmenH$_2$][Er(HCOO)$_4$]$_2$ (tmenH$_2^{2+}$ = N,N,N′,N′-tetramethylethylenediammonium). The transition is first-order and is accompanied by a unit cell volume change of about 10 %. High-pressure single-crystal X-ray diffraction studies reveal the complex bond rearrangement through the transition. The reversible nature of the transition is confirmed by means of independent nanoindentation measurements on single crystals.*

Pressure-induced phase transformations (PIPTs) can occur in a wide range of materials and are thus of great interest in a number of fields, such as chemistry, materials science, and geophysics.[1] In general, the bonding characteristics of the parent and the product phases of PIPT remain invariant in conventional materials, while new chemical bond formation with PIPT is reported in only a handful of cases.[2–8] Even in such instances, the bond rearrangement is usually irreversible owing to the substantial strain induced under pressure; the few exceptions involve relatively minor changes.[6–8] For example, Crain et al. reported that silicon undergoes a reversible pressure-induced structural transformation to give a different polymorph by simple dimerization of Si atoms in the unit cell,[6] and Olsen et al. reported a similar phenomenon involving bond migration in $Pb_3Bi_2S_6$.[7] In 2009, Goodwin et al. showed that $Ag_3[Co(CN)_6]$ undergoes a reversible structural transition under pressure in which compression induces alterations in the strength of the argentophilic interactions.[8]

Recent investigations of the mechanical properties of metal–organic frameworks (MOFs) and coordination polymers show that they are considerably more flexible than their inorganic or organic counterparts, because the metal polyhedra, bridged by the organic ligands, can rotate or relax more easily in response to external stimuli.[9] For example, the ferroelastic MOF perovskite, $[(CH_2)_3NH_2][Mn(HCOO)_3]$, can accommodate a lattice strain of about 5 % through an orthorhombic to monoclinic transition.[10] The flexibility of MOFs and coordination polymers can allow bond rearrangements to occur when they are compressed under hydrostatic pressure. This has been observed in the 1D coordination polymer $[CuF_2(H_2O)_2(pyridine)]$[11] and dense zeolitic imidazolate framework (ZIF), $[Zn(im)_2]$ (ZIF-zni, im = imidazolate),[12] though in the later the structural alteration is irreversible. In the present work, we show that the erbium formate framework, [tmenH$_2$][Er(HCOO)$_4$]$_2$ (**1**), is a rare example of a material that can undergo a reversible PIPT. By high-pressure single-crystal X-ray diffraction (HPSCXRD) studies, we establish that in this case PIPT is associated with a striking and complex bond rearrangement mechanism. Complementary nanoindentation measurements support the observations made in the X-ray studies.

Framework **1** crystallizes under ambient conditions in the monoclinic space group *C*2/*c* and has a pillared-layered 3D anionic $[Er(HCOO)_4]^-$ framework structure with channels in which the tmenH$_2^{2+}$ cations are located (Figure 1 a–d).[13] In each asymmetric unit of **1**, there is one Er^{3+}, four formate ligands, and half a tmenH$_2^{2+}$ cation (Supporting Information, Figure S1a). The Er^{3+} is eight-coordinate; each ErO_8 polyhedron is connected to five neighboring Er atoms by five $HCOO^-$ bridges to form the Er formate layers that lie parallel to the *bc* plane, while adjacent layers are pillared parallel to the *a*-axis by a sixth $HCOO^-$ bridge (Figure 1 c; Supporting Information, Figure S1). By omitting the tmenH$_2^{2+}$ guests, the structure can be simplified to a 6-connecting uninodal *vmd* net (Schäfli symbol $3^3{\cdot}4^5{\cdot}5^6{\cdot}6$),[14] as illustrated in Figure 1 d.

Figure 2 shows the evolution of the unit cell parameters of **1** as a function of pressure, which reveal the occurrence of

[*] Dr. W. Li,[+] Prof. A. K. Cheetham
Department of Materials Science and Metallurgy
Cambridge University
Charles Babbage Road, Cambridge, CB3 0FS (UK)
E-mail: wl276@cam.ac.uk
akc30@cam.ac.uk
Dr. E. C. Spencer,[+] Prof. N. L. Ross
Department of Geosciences, Virginia Tech
Blacksburg, VA, 24061 (USA)
Dr. M. S. R. N. Kiran,[+] Prof. U. Ramamurty
Department of Materials Engineering, Indian Institute of Science
Bangalore 560012 (India)
E-mail: satwiku@gmail.com
Prof. U. Ramamurty
Center of Excellence for Advanced Materials Research
King Abdulaziz University, Jeddah 21589 (Saudi Arabia)
[+] These authors contributed equally to this work.

[**] W.L. and A.K.C. acknowledge the European Research Council for providing financial support (Advanced Investigator Award to A.K.C.). N.L.R. and E.C.S. are grateful for support from the College of Science, Virginia Tech (U.S.A.) and support from NSF (EAR-1118691 awarded to N.L.R.). W.L. and M.S.R.N.K. thank Prof. Jodie Bradby of the Australian National University for the micro-Raman measurements.

Supporting information for this article is available on the WWW under http://dx.doi.org/10.1002/anie.201310276.

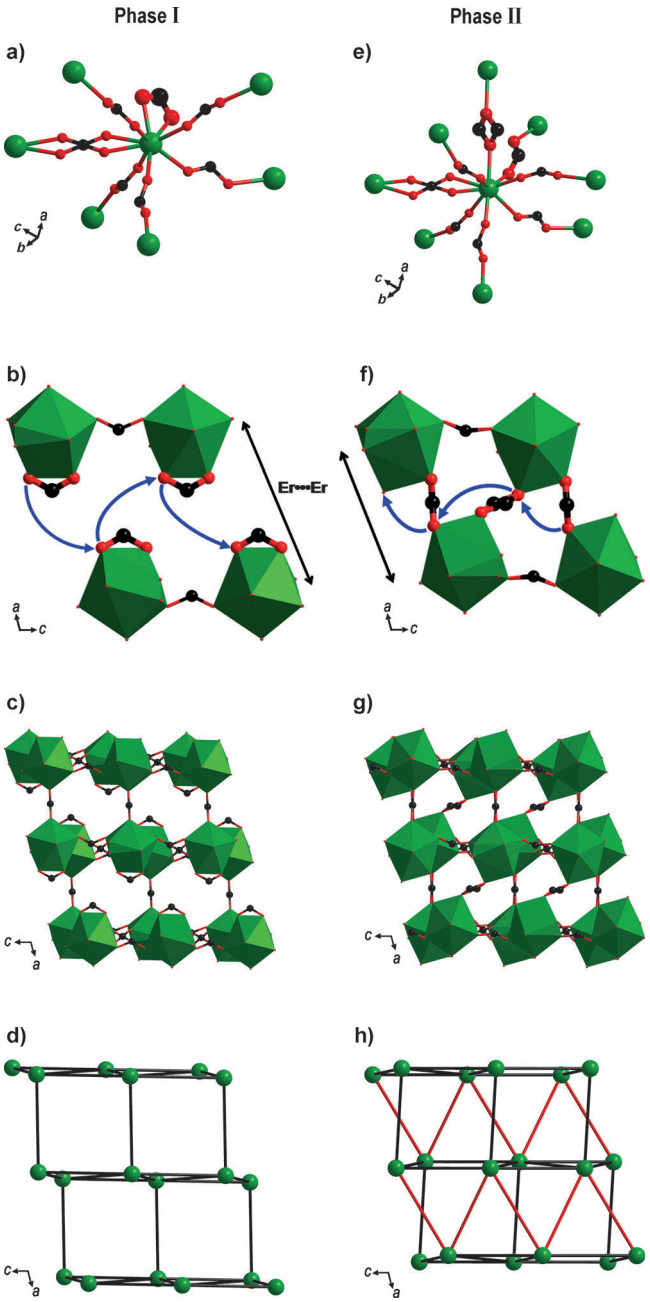

Figure 1. a), e) Coordination sphere for the Er^{3+} ions; b), f) phase transformation process; c), d), g), h) framework structure viewed along the *b*-axis and connectivity of the erbium centers in framework **1** at ambient pressure and 3.524(9) GPa. The $tmen^{2+}$ guests and hydrogen atoms are omitted for clarity. In (d) and (h), black struts represent Er–(HCOO)–Er links that lie approximately within the *bc* plane and generate a sheet motif, and parallel to the *a*-axis and act as pillars between neighboring sheets. Red struts show the new linkages that are formed as the crystal converts from phase I into II. The formate ligands, which change from a chelating mode in phase I to an *anti–anti* bridging coordination mode after the transition (phase II), have been enlarged and the bond rearrangement is indicated by arrows. Er^{3+} green, O red, C black, N blue.

a first-order phase transition at about 0.6 GPa. The crystal retains its monoclinic symmetry and space group *C*2/*c* through the phase transformation. However, there are significant differences in the unit cell parameters of phases I and II (Figure 2; Supporting Information, Figure S2, Tables S1, S2). The unit cell volume of Phase II at 0.855(4) GPa is about 10% smaller than that of phase I. The length of the *a*-axis undergoes a pronounced reduction of about 11% through the phase transition, while *b*- and *c*-axes expand by about 0.5 and 0.7%, respectively.[2] The volume–pressure (*V*-*P*) data for both phases were fit with second-order Birch–Murnaghan (BM) equations of state (EoS) (Supporting Information, Figure S2a) and the isothermal bulk moduli (K_0) for phases I and II were found to be 13.8(4) and 31.5(6) GPa, respectively. These values lie within the broad range of bulk moduli reported for other MOFs (ca. 6–30 GPa).[9] The significant difference in the compressibilities ($1/K_0$) of the two phases (0.072(2) and 0.0317(6) GPa^{-1} for phases I and II, respectively) indicate that the phase transition occurs through extensive alteration to the framework structure. Importantly, the transition is reversible, albeit with a small hysteresis. The isothermal axial compressibilies (β) for the unit cell axes of phases I and II are provided in Table 1. For phase I, the *a*-axis displays the greatest degree of

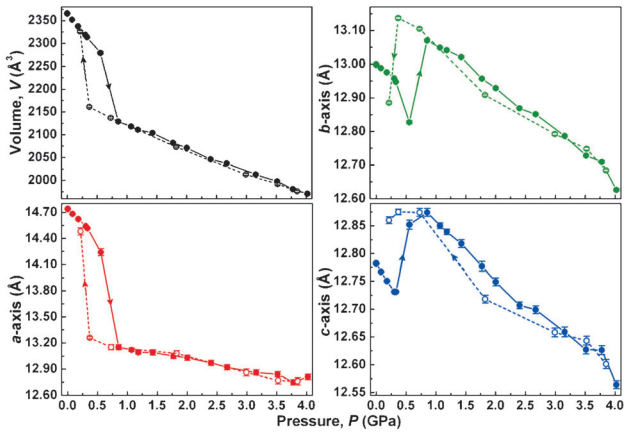

Figure 2. The unit cell parameters of framework **1** as a function of pressure. Over the pressure range investigated, $\alpha = \gamma = 90°$. Note: The data collected with increasing and decreasing pressure are plotted with filled and empty spheres respectively. The lines are there to guide the eye and the reversibility of the PIPT is indicated by arrows. A plot of the β-angle as a function of pressure, and the second order BM EoS fits are shown in the Supporting Information, Figure S2. The axial compressibility values reported in Table 1 were calculated from these fits.

Table 1: Isothermal axial compressibilities for phases I and II of framework **1**.

Orientation	Phase I [GPa^{-1}]	Phase II [GPa^{-1}]
β_a	$4.9(2)\times10^{-2}$	$1.24(9)\times10^{-2}$
β_b	$1.09(2)\times10^{-2}$	$1.33(5)\times10^{-2}$
β_c	$1.38(4)\times10^{-2}$	$8.8(3)\times10^{-3}$

compressibility, confirming that the structure is most easily deformed in the direction perpendicular to the erbium formate sheets that lie within the *bc* plane and is significantly more rigid along these sheets. As seen in Figure 1 d, e, only half of the Er^{3+} ions within each Er formate layer are pillared by formate bridges to the neighboring layer. This implies that

these Er^{3+} ions are less connected in this direction compared with the denser connectivity within the *bc* plane. As the Er—O and Er···Er distances in both the layers and the pillars are similar, the less linked *a*-axis orientation tends to be considerably more compressible.

X-ray data, collected at 1.070(5) and 3.524(9) GPa, were utilized for determining the structure of phase II of framework **1**. The most prominent difference between phases I and II is that the chelating formate groups bound to the Er^{3+} ions in phase I convert to bridging μ^2-ligands connecting neighboring Er^{3+} ions in phase II, though they are eight-coordinated in both phases (Figure 1 a,b and e,f). Consequently, additional linkages between adjacent Er^{3+} atoms along the *a*-axis are formed and the number of neighboring Er^{3+} ions linked to each Er^{3+} ion increases from six (phase I) to eight (phase II; Figure 1 a and e). This gives rise to a new 8-connecting *vmt* net with the Schäfli symbol $3^6{\cdot}4^{14}{\cdot}5^8$ (Figure 1 h). The bond rearrangement going from I to II is illustrated by the arrows in Figure 1 b and f; it is reminiscent of an on–off mechanism. This rearrangement results in a reduction from about 8.3 (ambient) to about 6.6 Å (1.070(5) GPa) in the distance between the two Er^{3+} ions that lie opposite the chelating formate ligands in phase I. These additional linkages reinforce the cross-linking between adjacent Er formate sheets in phase II and in turn reduce the interlayer distance by about 0.8 Å. As there are two interlayer spaces per unit cell, a difference (Δa) of about 1.6 Å between phases I (ambient pressure) and II (at 1.070(5) GPa) is expected, and indeed this is apparent in the unit cell versus pressure data (Figure 2; Supporting Information, Figure S2). The additional formate linkages between adjacent layers in phase II are also the reason for the enhanced structural rigidity and larger bulk modulus of this phase relative to phase I. The expansion in the *bc* plane that accompanies the phase transition is facilitated by distortions and subtle changes in the orientations of the Er^{3+} polyhedra. We do not believe that the $tmenH_2^{2+}$ cation plays a significant role in the transformation, as it is weakly hydrogen-bonded to the framework. It is important to highlight that the flexible coordination geometry of the erbium polyhedra plays a crucial role in the transformation by allowing a structural rearrangement to occur without leading to framework collapse.[15] These major modifications in the coordination environments of the Er^{3+} ions are further evidenced by splitting of the 552.5 nm fluorescence emission signal of framework **1** at pressures in excess of 0.6 GPa (Supporting Information, Figure S3).

Most MOF structures respond to pressure by rotating the metal polyhedra and/or flexing the metal–ligand "hinges".[12,15–23] Thus, it is unusual for this class of materials to exhibit significant changes in bond lengths in response to pressure. Framework **1** conforms to this trend in that the Er—O bond lengths do not change (within error) between phases I and II. To date, there has been only one published example of a MOF undergoing pressure-induced cooperative bond rearrangement, as mentioned above.[12] The framework $[Zn(im)_2]$ (ZIF-zni) undergoes a phase transition at about 0.7 GPa during which the bridging imidazolate anions reorganize, a process that necessitates the breaking and reformation of Zn—N bonds. However, unlike framework **1**, the ZIF-zni phase transition is irreversible.

We employed the nanoindentation technique to provide further corroborative evidence for PIPT in **1**.[9,24] In the recent past, the ability of nanoindentation to reflect PIPTs with signature discontinuity events in the load-depth of penetration (*P–h*) curves, such as "pop-in" during loading and "pop-out", "kink", or "elbow" formation during unloading, has been established fairly well.[25–27] Representative *P–h* curves obtained on the {100} and {001} faces of crystals of **1** with a spherical tipped indenter (tip radius ca. 10 μm) are displayed in Figure 3. Several features are noteworthy:

1) The resistance to the penetration of the indenter is much higher on {001} than on {100}. This anisotropy in the elastic response is due to arrangement of the pillar-layered structure of **1**, which has been discussed above. Detailed description and analysis are included in the ESI (Supporting Information, Figures S4, S5).
2) Both the loading parts of the *P–h* curves contain subtle but highly reproducible (Supporting Information, Figures S6, S7) undulations; instantaneous slopes of the *P–h* curves (d*P*/d*h*) are plotted against *h* in the insets of Figure 3 to accentuate these features. Similar discontinuities are reported during indentation loading of Si and were attributed to the transformation from the diamond Si-I structure to the metallic β-tin Si-II phase.[25,28] As pop-ins in MOFs are not due to fracture, they could be correlated to phase change underneath the indenter.[9,29] The reproducibility and similarity of features with those of the literature suggests that the observed undulations could be attributed to Phase I→II transformation during loading. The estimated pressures for the onset of the PIPT during loading are about 0.17 and about 0.32 GPa on the {100} and {001} faces, respectively (Supporting Information, Figure S8),[30,31] which are lower than the transformation pressure (ca. 0.6 GPa) under hydrostatic con-

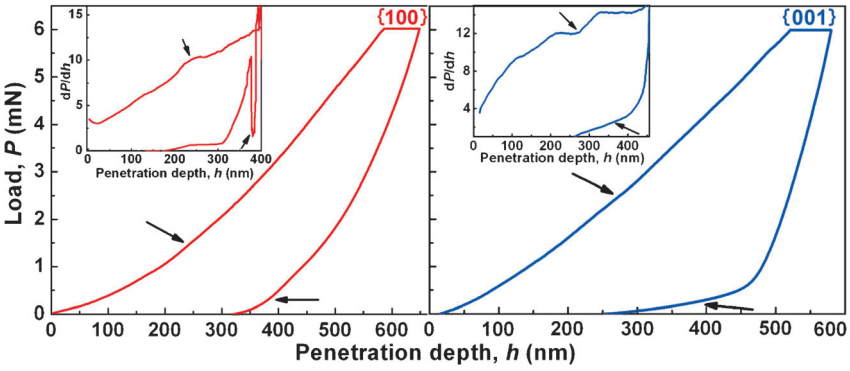

Figure 3. Representative *P–h* curves for **1** obtained from indentation with a spherical tip normal to the {100} and {001} facets. Inset: The derivative of the loading and unloading curves as a function of penetration depth for the weak "kink" and strong "elbow" events. The anomalies seen during loading and unloading are indicated with arrows.

ditions. This disparity can be due to the fact that the stress state underneath the indenter contains a significant amount of shear in addition to the hydrostatic component and can thus induce the PIPT more easily.[25,32,33]

3) A subtle "S" shape and a sudden and marked reduction are seen in the unloading segments at a load of about 0.25 mN for {100} and at about 0.40 mN for {001}, respectively. Again these features are not only highly reproducible (Supporting Information, Figures S6, S7) but are also akin to the weak "kink"- and a strong "elbow"-like features reported in literature for other inorganic solids that undergo PIPT during indentation.[34–36] These features, which occur during unloading, are attributed to the indenter tip being pushed up by volume expansion that occurs during the phase II→I transformation, consistent with the significant unit cell volume change (ca. 10%) observed by HPSCXRD.

To examine the reversible nature of the PIPT induced by indentation, micro-Raman spectroscopy was performed on the residual indentation imprints. These spectra match well with those obtained prior to indentation (Supporting Information, Figure S9), and neither a shift of the peaks nor new peaks are seen, confirming the reversible nature of the indentation-induced PIPT, which is consistent with the results from the X-ray studies.

In summary, we have employed high-pressure X-ray diffraction and nanoindentation techniques to study a pressure-induced phase transition in the pillar-layered MOF material, $[tmenH_2^{2+}][Er(HCOO)_4]_2$ (**1**). X-ray studies reveal that the first-order phase transformation at about 0.6 GPa is reversible and associated with striking bond rearrangements. Furthermore, both the loading and unloading load-penetration curves obtained through nanoindentation on {100} and {001} facets of the MOF single crystals show features that reflect the reversibility of the transition, thus providing independent evidence of the pressure-induced phase transformation.

Received: November 26, 2013
Revised: January 17, 2014
Published online: April 7, 2014

Keywords: bond rearrangement · high-pressure X-ray diffraction · metal–organic frameworks · nanoindentation · pressure-induced phase transformations

[1] Z. Sun, J. Zhou, H.-K. Mao, R. Ahuja, *Proc. Natl. Acad. Sci. USA* **2012**, *109*, 5948 – 5952.
[2] W. Cai, A. Katrusiak, *J. Phys. Chem. C* **2013**, *117*, 21460 – 21465.
[3] S. H. Lapidus, G. J. Halder, P. J. Chupas, K. W. Chapman, *J. Am. Chem. Soc.* **2013**, *135*, 7621 – 7628.
[4] W. Paraguassu, M. Maczka, A. G. Souza Filho, P. T. C. Freire, J. Mendes Filho, J. Hanuza, *Phys. Rev. B* **2010**, *82*, 17410.
[5] S. Li, Q. Li, K. Wang, M. Zhou, X. Huang, J. Liu, K. Yang, B. Liu, T. Cui, G. Zou, B. Zou, *J. Phys. Chem. C* **2013**, *117*, 152 – 159.
[6] J. Crain, G. J. Ackland, J. R. Maclean, R. O. Piltz, P. D. Hatton, G. S. Pawley, *Phys. Rev. B* **1994**, *50*, 13043 – 13046.
[7] L. A. Olsen, T. Balić-Žunić, E. Makovicky, *Inorg. Chem.* **2008**, *47*, 6756 – 6762.
[8] A. L. Goodwin, D. A. Keen, M. G. Tucker, *Proc. Natl. Acad. Sci. USA* **2008**, *105*, 18708 – 18713.
[9] J.-C. Tan, A. K. Cheetham, *Chem. Soc. Rev.* **2011**, *40*, 1059 – 1080.
[10] W. Li, Z. Zhang, E. G. Bithell, A. S. Batsanov, P. T. Barton, P. J. Saines, P. Jain, C. J. Howard, M. A. Carpenter, A. K. Cheetham, *Acta Mater.* **2013**, *61*, 4928 – 4938.
[11] A. Prescimone, C. Morien, D. Allan, J. A. Schlueter, S. W. Tozer, J. L. Manson, S. Parsons, E. K. Brechin, S. Hill, *Angew. Chem.* **2012**, *124*, 7608 – 7612; *Angew. Chem. Int. Ed.* **2012**, *51*, 7490 – 7494.
[12] E. C. Spencer, R. J. Angel, N. L. Ross, B. E. Hanson, J. A. K. Howard, *J. Am. Chem. Soc.* **2009**, *131*, 4022 – 4026.
[13] M. Li, B. Liu, B. Wang, Z. Wang, S. Gao, M. Kurmoo, *Dalton Trans.* **2011**, *40*, 6038 – 6046.
[14] The reticular code was analyzed using TOPOS 4.0 software: http://www.topos.ssu.samara.ru/.
[15] J. M. Ogborn, I. E. Collings, S. A. Moggach, A. L. Thompsona, A. L. Goodwin, *Chem. Sci.* **2012**, *3*, 3011 – 3017.
[16] A. J. Graham, D. R. Allan, A. Muszkiewicz, C. A. Morrison, S. A. Moggach, *Angew. Chem.* **2011**, *123*, 11334 – 11337; *Angew. Chem. Int. Ed.* **2011**, *50*, 11138 – 11141.
[17] M. Mattesini, J. M. Soler, F. Ynduráin, *Phys. Rev. B* **2006**, *73*, 094111.
[18] W. Li, M. R. Probert, M. Kosa, T. D. Bennett, A. Thirumurugan, R. P. Burwood, M. Parinello, J. A. K. Howard, A. K. Cheetham, *J. Am. Chem. Soc.* **2012**, *134*, 11940 – 11943.
[19] E. C. Spencer, N. L. Ross, R. J. Angel, *J. Mater. Chem.* **2012**, *22*, 2074 – 2080.
[20] I. E. Collings, A. B. Cairns, A. L. Thompson, J. E. Parker, C. C. Tan, M. G. Tucker, J. Catafesta, C. Levelut, J. Haines, V. Dmitriev, P. Pattison, A. L. Goodwin, *J. Am. Chem. Soc.* **2013**, *135*, 7610 – 7620.
[21] K. J. Gagnon, C. M. Beavers, A. Clearfield, *J. Am. Chem. Soc.* **2013**, *135*, 1252 – 1255.
[22] S. A. Moggach, T. D. Bennett, A. K. Cheetham, *Angew. Chem.* **2009**, *121*, 7221 – 7223; *Angew. Chem. Int. Ed.* **2009**, *48*, 7087 – 7089.
[23] T. D. Bennett, P. Simoncic, S. A. Moggach, F. Gozzo, P. Macchi, D. A. Keen, J. C. Tan, A. K. Cheetham, *Chem. Commun.* **2011**, *47*, 7983 – 7985.
[24] S. Varughese, M. S. R. N. Kiran, U. Ramamurty, G. R. Desiraju, *Angew. Chem.* **2013**, *125*, 2765 – 2777; *Angew. Chem. Int. Ed.* **2013**, *52*, 2701 – 2712.
[25] V. Dominich, Y. Gogotsi, *Rev. Adv. Mater. Sci.* **2002**, *3*, 1 – 36.
[26] A. P. Gerk, D. Tabor, *Nature* **1978**, *271*, 732 – 733.
[27] U. Ramamurty, J. Jang, *CrystEngComm* **2014**, *16*, 12 – 23.
[28] J. E. Bradby, J. S. Williams, J. Wong-Leung, M. V. Swain, P. Munroe, *J. Mater. Res.* **2001**, *16*, 1500 – 1507.
[29] J.-C. Tan, C. A. Merrill, J. B. Orton, A. K. Cheetham, *Acta Mater.* **2009**, *57*, 3481 – 3496.
[30] W. C. Oliver, G. M. Pharr, *J. Mater. Res.* **1992**, *7*, 1564 – 1583.
[31] N. Iwashita, M. V. Swain, J. S. Field, N. Ohta, S. Bitoh, *Carbon* **2001**, *39*, 1525 – 1532.
[32] S. S. Bhat, U. V. Waghmare, U. Ramamurty, *J. Appl. Phys.* **2013**, *113*, 133507.
[33] J. J. Gilman, *Mater. Res. Soc. Symp. Proc.* **1992**, *276*, 191 – 196.
[34] T. Juliano, Y. Gogotsi, V. Dominich, *J. Mater. Res.* **2003**, *18*, 1192 – 1201.
[35] T. Juliano, Y. Gogotsi, V. Dominich, *J. Mater. Res.* **2004**, *19*, 3099 – 3108.
[36] J. Jang, M. J. Lance, S. Wen, T. Y. Tsui, G. M. Pharr, *Acta Mater.* **2005**, *53*, 1759 – 1770.

